

Electronic Supplementary Information:

Predicting the reactivity of energetic materials: an ab initio multi-phonon approach

*Adam A.L. Michalchuk,^{*1,2} Peter Portius,³ Morris Trestman,¹ Svemir Rudić,⁴ Peter T. Fincham,⁵ Colin R. Pulham^{1,2*} and Carole A. Morrison.^{1*}*

1. EaStCHEM School of Chemistry and Centre for Science at Extreme Conditions, University of Edinburgh, Edinburgh, UK. 2. EPSRC Centre for Continuous Manufacturing and Crystallisation (CMAC), University of Edinburgh, Edinburgh, UK. 3. Department of Chemistry, University of Sheffield, Western Bank, Sheffield S3 7HF, U.K. 4. ISIS Neutron and Muon Source, STFC, Rutherford Appleton Laboratory, Chilton, Didcot, UK. 5. Defence Science and Technology Laboratory (DSTL), Porton Down, Salisbury SP4 0JG, Wiltshire, U.K.

Contents

S1. Crystal structures of energetic materials	2
S2. Calculated unit cell parameters	3
S3. Vibrational spectra of energetic materials	4
S4. Inelastic neutron scattering spectroscopy convergence	7
S5. Numerical example of doorway density calculations	9
S6. The projected phonon density of states, $P(\Omega^{(2)})$	10
S7. Overtone coupling calculations	11
S8. Overtone calculations at higher order coupling.....	12
S9 Vibrational modes of TATB and HNB.....	13
S10. References	15

1. Crystal structures of energetic materials

The unit cell for each of the EMs used through this work is given in Figure S2.1. Data for literature structures are taken from the Cambridge Crystallographic Data Centre (CCDC), corresponding to: β -HMX (Ref: OCHTET15¹), α -FOX-7 (Ref: SEDTUQ03²), NTO (Ref: QOYJOD06³), HNB (Ref: HNOBEN⁴), ABT (Ref: EWEYEL⁵), HBT (Ref: TIPZAU⁶), TATB (Ref: TATNBZ⁷), DNIT (Ref: VIWRAV⁸), MNT (Ref: VITBAC⁸), GTZ (CSD Deposition 1900007), AGTZ (CSD Deposition 1900008), DGTZ (CSD Deposition 1900009), ATZ (Ref: EJIQEU01)

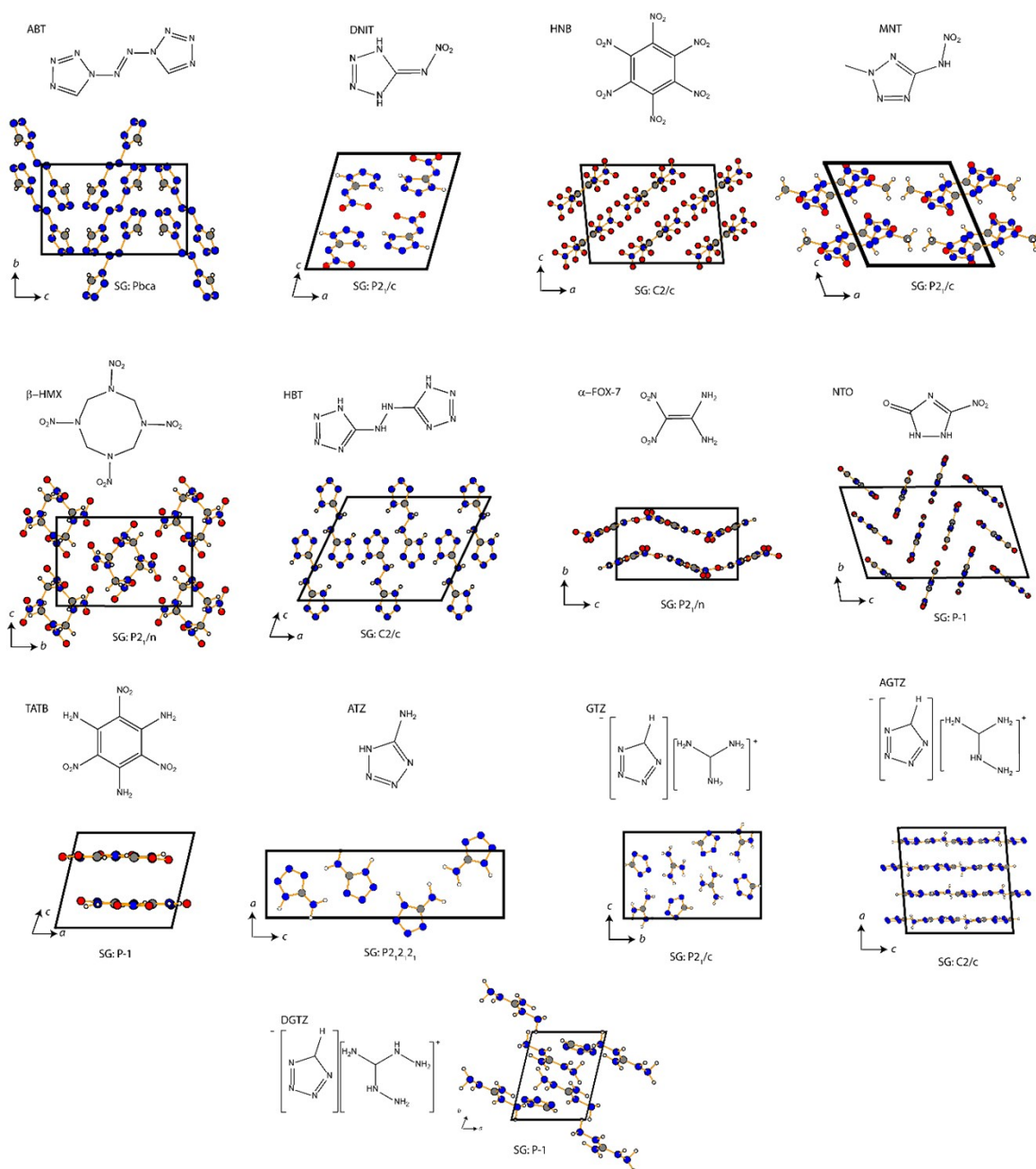


Figure S1.1: Unit cell structure for each EM used in this work. The cell axes are indicated along with space group (SG). Atoms are colored according to: White- hydrogen; Grey- carbon; Blue- nitrogen; Red- oxygen.

2. Calculated unit cell parameters

Prior to calculation of the phonon dispersion curves, all structures were relaxed. The resulting, relaxed unit cell parameters are given in Table S2.1 and compared to input experimental parameters. Note that where applicable, DFT calculations were performed on the primitive unit cell structures. All DFT structures are compared to low temperature experimental data, where available.

Table S2.1: Comparison of unit cell parameters from DFT calculations (*calc*) against experimental parameters (*exp*). The space group (SG) is given for each experimental structure, and remains unchanged upon relaxation. For non-primitive cells, the corresponding parameters of the primitive cell are also given. The total change in volume (dV) is given for each relaxed structure.

	SG	a	b	c	α	β	γ	V	dV/%
ABT ^{exp}	<i>Pbca</i>	8.352	6.793	11.614	90	90	90	658.962	
ABT ^{calc}		8.354	6.789	11.618	90	90	90	658.931	-0.004%
DNIT ^{exp}	<i>P2₁/c</i>	9.401	5.492	9.315	90	105.762	90	462.835	
DNIT ^{calc}		9.413	5.526	9.758	90	105.317	90	489.546	+5.77%
HNB ^{exp}	<i>C2/c</i>	13.220	9.130	9.680	90	95.500	90	581.490	
HNB ^{exp}	<i>P(C2/c)</i>	9.046	9.046	9.680	62.280	62.280	60.620	581.492	
HNB ^{calc}		9.028	9.028	9.771	62.444	62.444	59.981	582.977	+0.26%
MNT ^{exp}	<i>P2₁/c</i>	9.528	7.731	8.460	90	112.875	90	574.122	
MNT ^{calc}		9.644	7.771	8.612	90	113.203	90	593.209	+3.32%
β -HMX ^{exp}	<i>P2₁/c</i>	6.525	11.024	7.362	90	102.642	90	516.675	
β -HMX ^{calc}		6.624	11.256	7.373	90	102.222	90	537.299	+4.00%
HBT ^{exp}	<i>C2/c</i>	12.401	5.513	9.835	90	115.570	90	606.565	
HBT ^{exp}	<i>P(C2/c)</i>	6.786	6.786	9.835	113.230	113.230	47.940	303.283	
HBT ^{calc}		6.706	6.706	9.724	111.837	111.837	49.440	303.075	-0.07%
α -FOX7 ^{exp}	<i>P2₁/n</i>	6.934	6.622	11.312	90	90.065	90	519.470	
α -FOX7 ^{calc}		7.089	6.623	11.440	90	91.273	90	530.898	+2.20%
NTO ^{exp}	<i>P-1</i>	5.123	10.314	17.998	106.610	97.810	90.130	902.060	
NTO ^{calc}		5.159	10.461	17.686	107.247	97.777	90.056	902.450	+0.04%
TATB ^{exp}	<i>P-1</i>	9.010	9.028	6.812	108.580	91.820	119.970	442.524	
TATB ^{calc}		9.128	9.142	6.767	109.012	92.097	119.936	448.784	+1.41%
ATZ ^{exp}	<i>P2₁2₁2₁</i>	5.090	3.666	18.0741	90	90	90	337.289	
ATZ ^{calc}		5.073	3.680	18.067	90	90	90	337.303	+0.004%
GTZ ^{exp}	<i>P2₁/c</i>	4.730	13.894	8.754	90.0	92.96	90.0	574.485	
GTZ ^{calc}		4.897	13.699	8.876	90	92.456	90	594.843	+3.54%
AGTZ ^{exp}	<i>C2/c</i>	12.602	8.012	12.778	90.0	94.529	90.0	1286.23	
AGTZ ^{exp}	<i>P(C2/c)</i>	7.467	7.467	12.778	93.821	93.821	64.893	643.114	
AGTZ ^{calc}		7.452	7.452	13.077	95.163	95.163	65.597	657.534	+2.24%
DGTZ ^{exp}	<i>P-1</i>	6.097	7.318	8.094	94.979	97.659	104.058	344.517	
DGTZ ^{calc}	<i>P-1</i>	6.085	7.308	8.236	92.978	98.824	102.677	351.731	+2.09%

3. Vibrational spectra of energetic materials

3.1. Phonon dispersion curves

The vibrational up-pumping model used in this work is based off integration over the complete Brillouin zone. The corresponding phonon dispersion curves were generated within the framework of Density Functional Perturbation Theory (DFPT) and are provided in Figure S3.1. To allow for ease of visualization, these data are provided to a maximum of 600 cm^{-1} .

Unfortunately, both NTO and HNB exhibit slight instabilities in the calculated dispersion curves; their lowest acoustic branch falls below zero at a number of points across the Brillouin zone). Noting that neither phase is metastable, it is assumed that these effects are numerical. Given the excellent agreement of the calculated INS spectrum (including integration across the complete Brillouin zone) against the experimental spectrum, Figure 3 (main text), we do not expect these small instabilities to have any major influence on the rest of the vibrational structure.

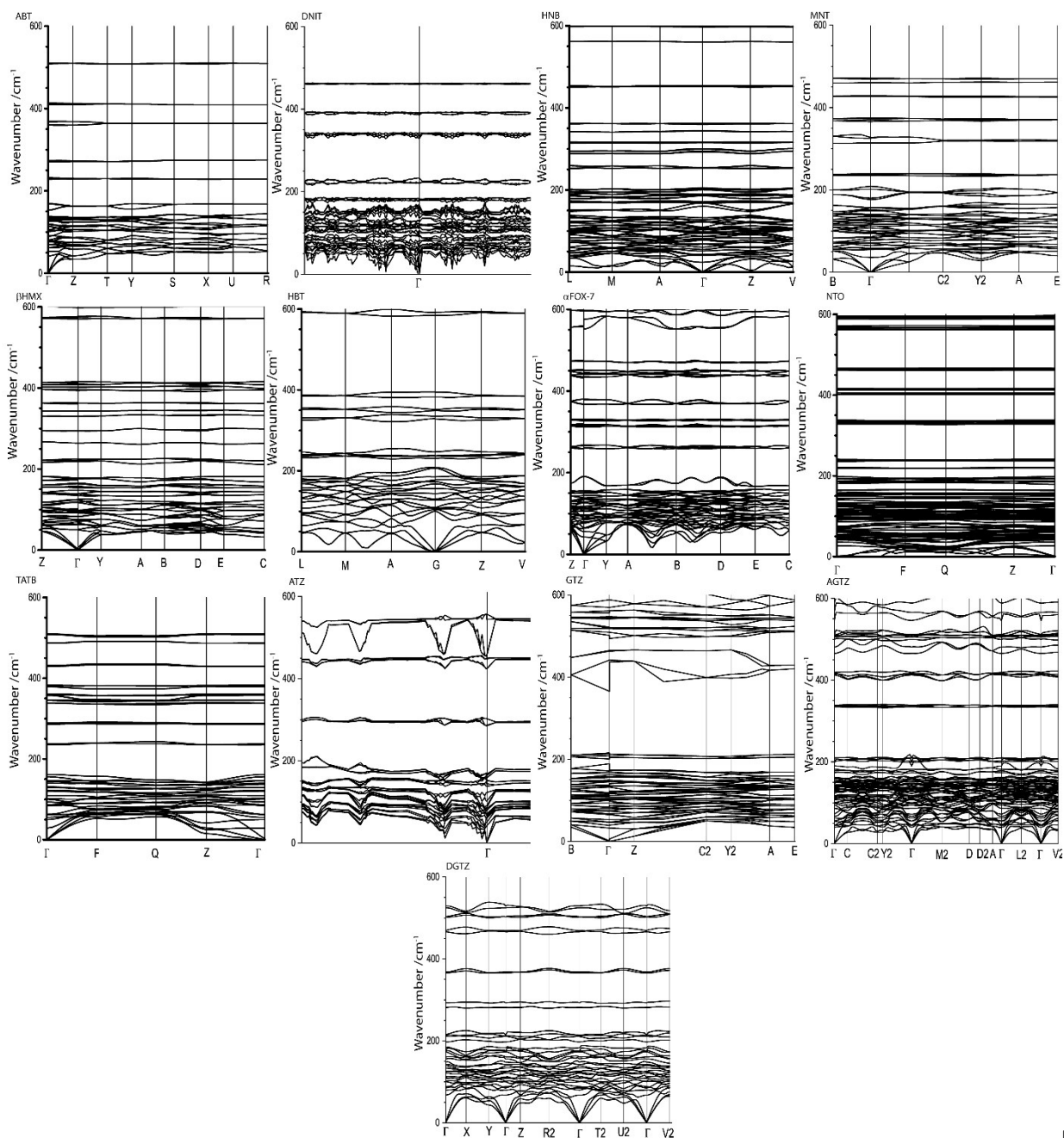


figure S3.1.1: Phonon dispersion curves for EMs used in this work. All curves are generated within the framework of DFPT, using the PBE GGA functional. Data are plotted across the high-symmetry lines as suggested by SeeKPath⁹, and labelled according to the international tables convention.

3.2. Phonon density of states

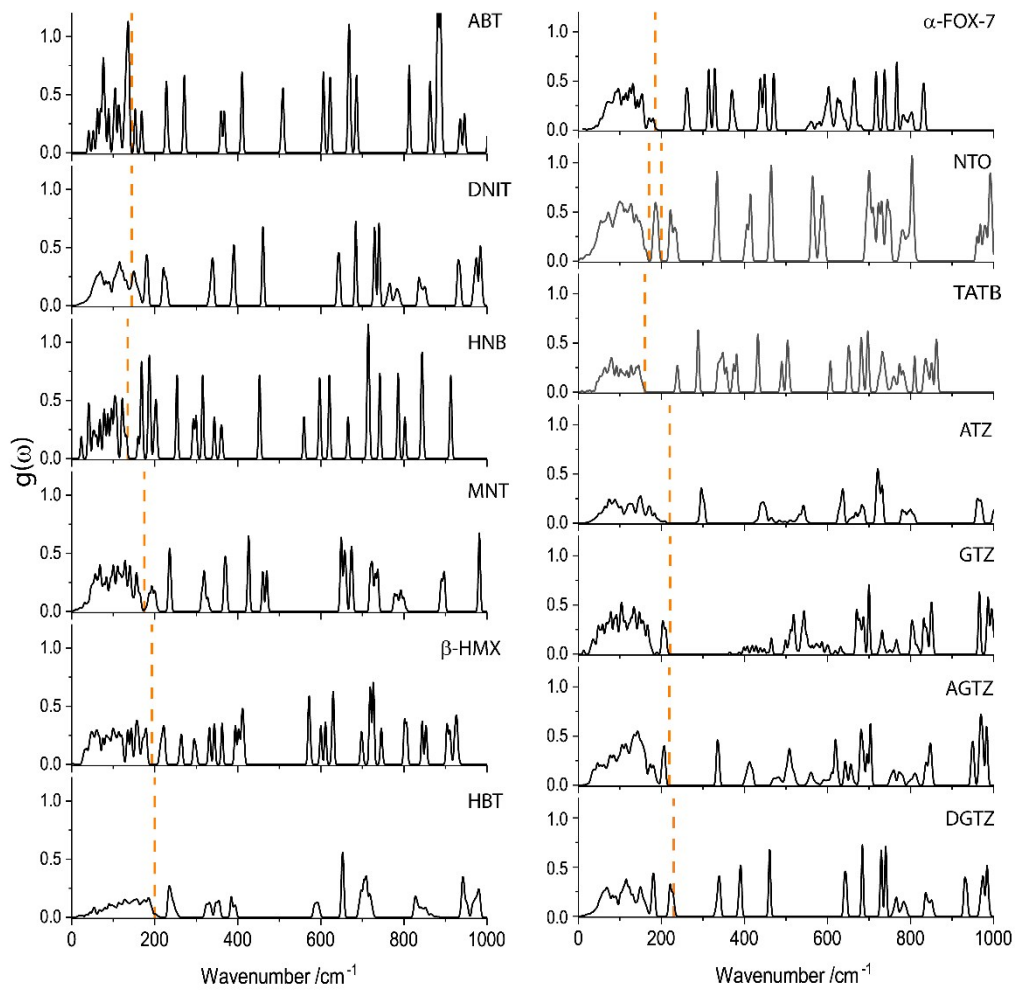


Figure S3.2.1: Calculated phonon density of states generated from integration across the first Brillouin zone. The values of Ω_{max} are indicated by vertical dotted lines. Gaussian smearing of 5 cm^{-1} is applied.

4. Inelastic neutron scattering spectroscopy convergence

In order to simulate INS spectra of the EMs used in this manuscript, the vibrational spectra were averaged over a series of q -point densities, Figure S4.1.1 and S4.1.2. While zone-centre ($q=0$) sampling is sufficient to obtain the correct frequencies, capturing the intensities requires a denser modelling grid. In all cases, sampling with density of approximately 0.08 \AA^{-1} yields good overall description of the experimentally determined spectra.

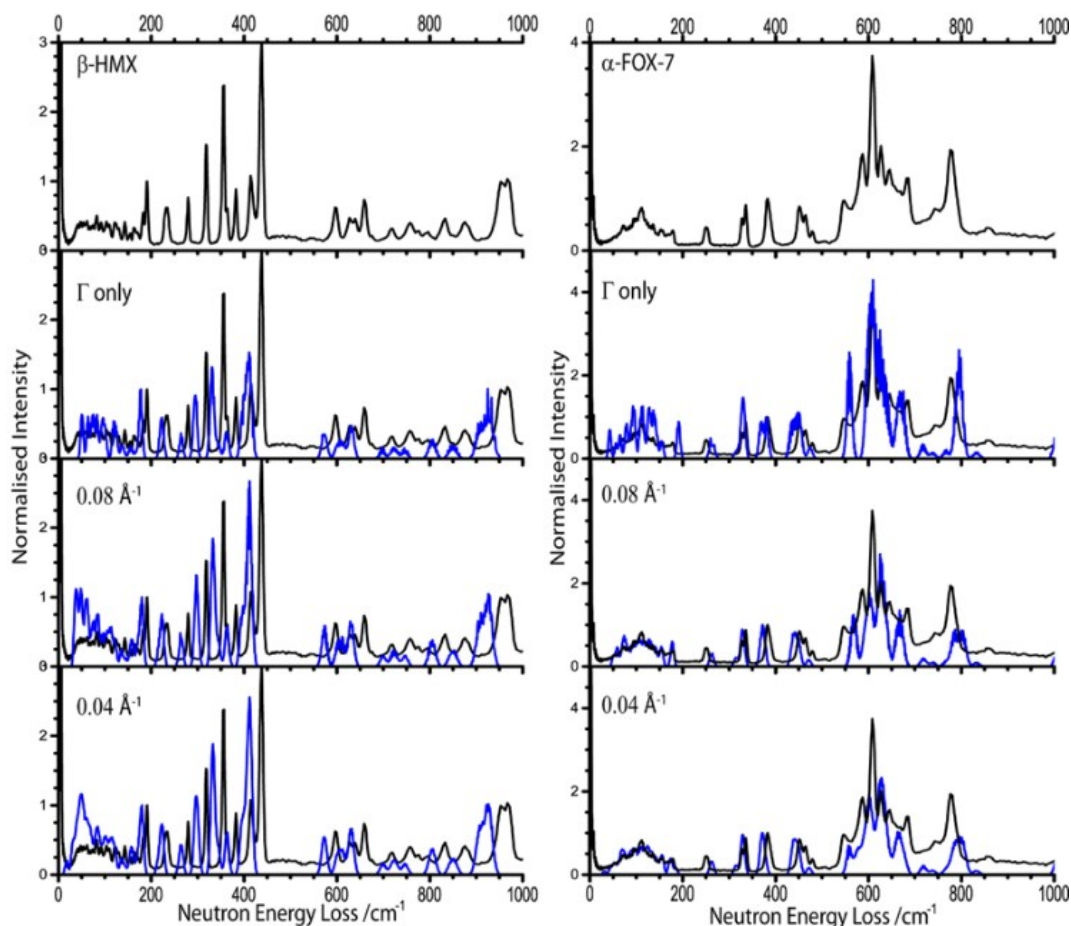


Figure S4.1.1: INS spectra for β -HMX and α -FOX-7 at 10 K. The experimental pattern (black lines) is shown in comparison to simulated INS spectra (blue lines) at sampling densities of the Brillouin zone Γ only, 0.08 \AA^{-1} and 0.04 \AA^{-1} .

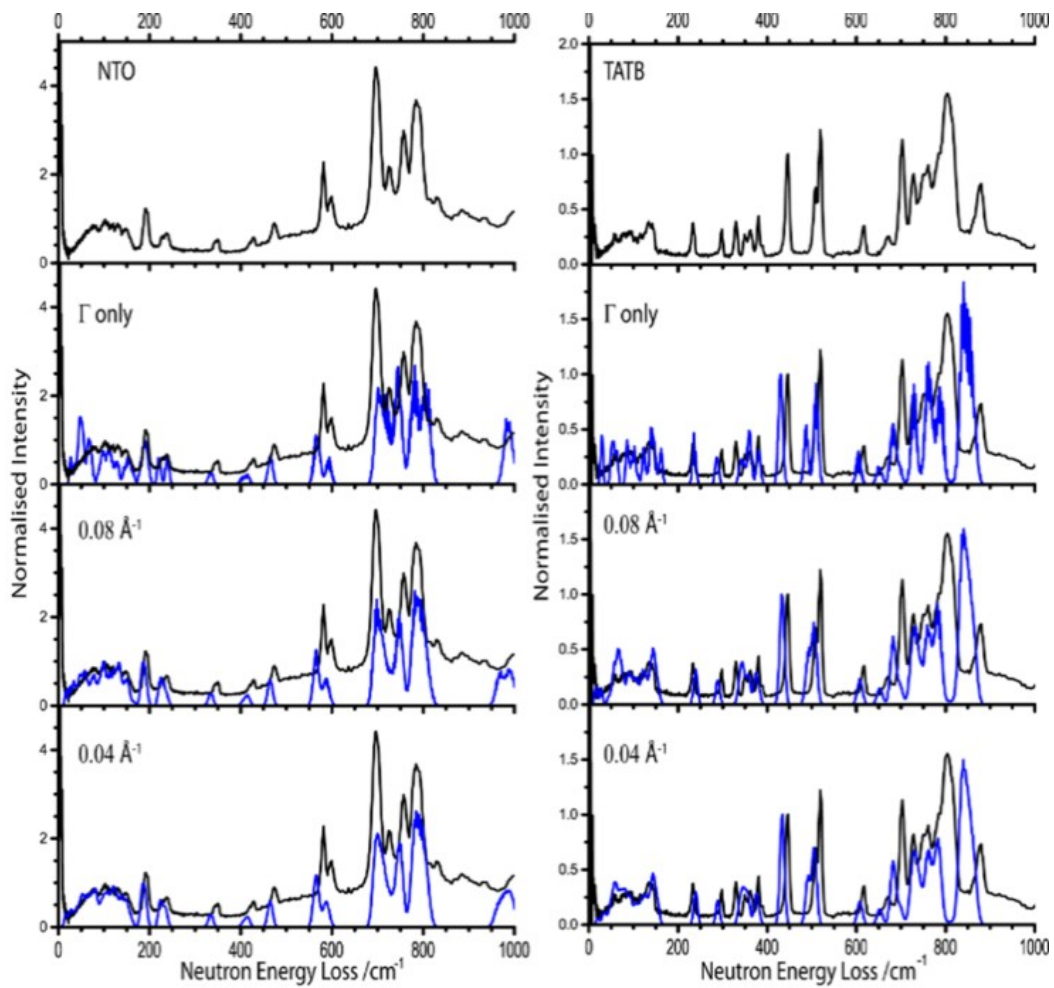


Figure S4.1.2: INS spectra for NTO and TATB at 10 K. The experimental pattern (black lines) is shown in comparison to simulated INS spectra (blue lines) at three different sampling densities of the Brillouin zone.

5. Numerical example of doorway density calculations

To simplify discussion of the density of doorway states presented in Figure 5 (main text) we present here a numerical example, based on two data points, HNB and TATB. We first note that the DOS presented in Figure S4.2.1 are normalized to $3N$ to reflect the total number of states present in the corresponding Brillouin zone.

For TATB, we define the doorway region from $\Omega_{max} = 160 \text{ cm}^{-1}$ until $2\Omega_{max} = 320 \text{ cm}^{-1}$. An integration of the TATB DOS over this region gives a total number of 6.07 states, $g(\omega)_D$. Consistent with the method described by Bernstein¹⁰, this density is normalized by the total number of available states (*i.e.* $g(\omega)_T = \int g(\omega)d\omega = 144.00$). Finally, the density of states in the doorway region is obtained by normalizing to the size of the respective doorway region, 160 cm^{-1} . Hence, we obtain the density of doorway states according to

$$DODS = \frac{g(\omega)_D}{g(\omega)_T \times \Omega_{max}} = \frac{6.07}{144.0 \times 160} = 2.63E - 4$$

The same calculation for HMX yields

$$DODS = \frac{g(\omega)_D}{g(\omega)_T \times \Omega_{max}} = \frac{14.07}{167.99 \times 193} = 4.34E - 4$$

The necessary values used to derive data in Figure 5 are given in Table S5.1. To assist visualization, all values in the main text are scaled by a factor of 10^4 .

Table S5.1: Calculation of doorway density presented in Figure 5 of main text.

	$\Omega_{max} / \text{cm}^{-1}$	$\int_{\Omega_{max}}^{2\Omega_{max}} g(\omega)d\omega$	$\int g(\omega)d\omega$
ABT	145	11.99904	167.91664
DNIT	145	12.18078	131.91624
HNB	135	20.00002	143.91297
MNT	175	11.96816	167.94535
HMX	193	14.07173	167.99123
HBT	200	10.20427	95.97982
FOX7	185	13.87112	167.99123
NTO	170	22.2286	247.02029
NTO	200	15.42819	247.02029
TATB	160	6.07258	144.00085
ATZ	220	5.28085	107.95298
GTZ	225	2.81791	191.70000
AGTZ	235	6.50151	179.8843
DGTZ	235	5.00528	119.94783

6. The projected phonon density of states, $P(\Omega^{(2)})$

If one requires inclusion of at least one phonon mode ($\omega < \Omega_{max}$), the two-phonon density of states is continuous while $\Delta\omega < \Omega_{max}$ is true of the fundamental structure. A subset of examples are given in Figure S6.1. Thus, many energies can be achieved than there are fundamental modes to accept them. It is therefore necessary to consider up-pumping only from multi-phonon states which are resonant with a fundamental band. This is achieved by projecting the $\Omega^{(2)}$ onto $g(\omega)$, Figure S6.2. Note that in doing so, most of the multi-phonon density is lost. This has significant consequence on the calculation of vibrational up-pumping.

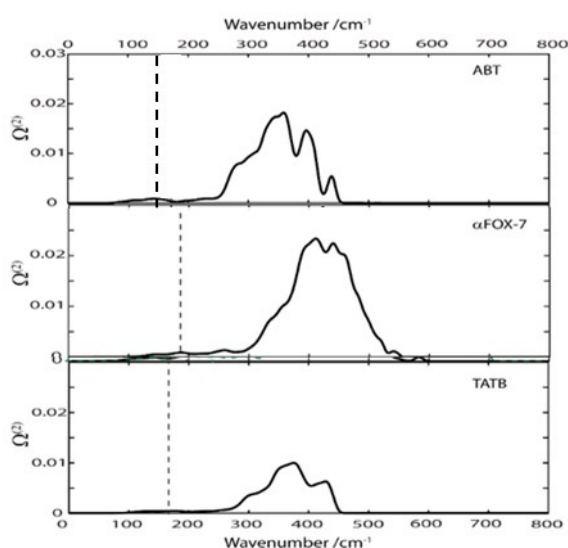


Figure S6.1: Example two-phonon density of states ($\Omega^{(2)}$). The values of Ω_{max} are indicated by vertical dotted lines.

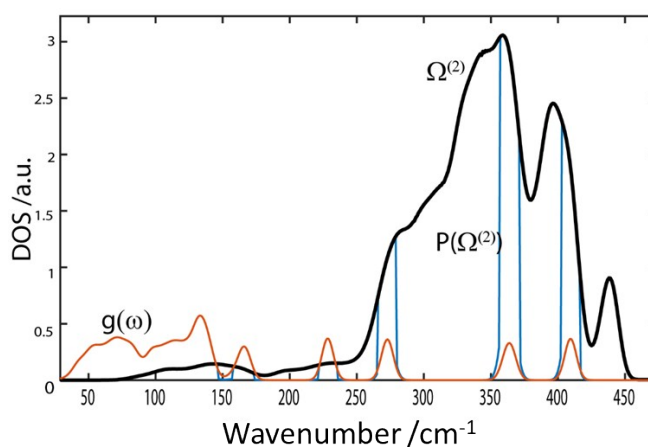


Figure S6.2: The full $\Omega^{(2)}$ for ABT (black), alongside the single phonon DOS $g(\omega)$ (orange) and the projection of $\Omega^{(2)}$ onto the DOS, $P(\Omega^{(2)})$ (blue).

7. Overtone coupling calculations

7.1. Numerical example of overtone coupling calculations

The calculation of the m^{th} -order overtone contribution follows from Equation 10 (main text),

$$g(\omega)^{(m)} = g(\omega)/(m + 1); \quad \omega^{(m)} = (m + 1) \times \omega$$

This leads to generation of a unique multi-phonon density of states for each overtone order. An example is shown in Figure S7.1

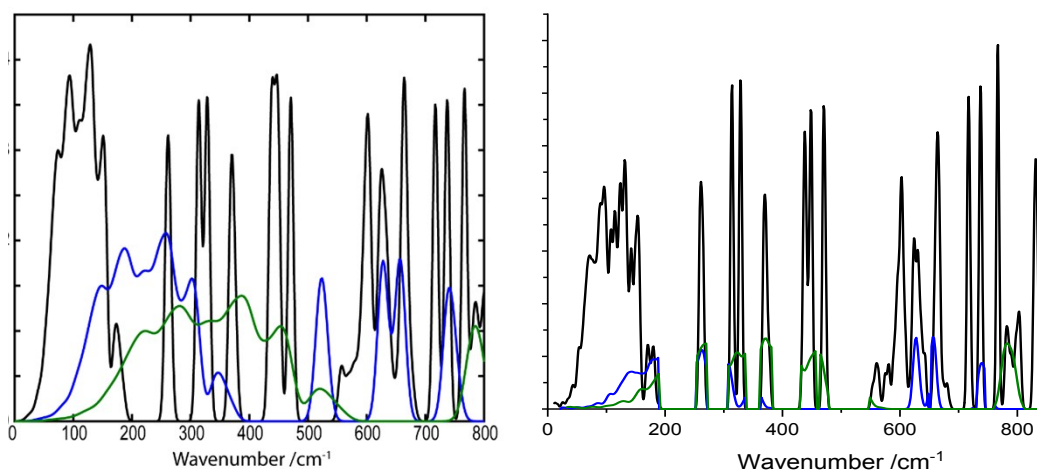


Figure 7.1: Overtone density of states. (left) The full overtone multi-phonon density of states are shown for (blue) $m=1$ and (green) $m=2$. (right) Projection of overtone density of states ($m=1$ and $m=2$ as blue and green, respectively) onto the fundamental structure.

To permit scaling between systems, the integral of $g(\omega)^{(1+2)}$ is divided by $\int g(\omega)d\omega$. The normalized values for each of $g(\omega)^{(1)}$ and $g(\omega)^{(2)}$ are given in Table S7.1

Table S7.1: Values of $g(\omega)^{(m)}$ normalised by $\int g(\omega)d\omega$ for each of the test systems used in this work.

System	$g(\omega)^{(m)}$		Total
	$m=1$	$m=2$	
ABT	4.22	2.91	7.13
DNIT	3.15	2.61	5.76
HNB	4.37	3.90	8.27
MNT	3.16	3.05	6.21
HMX	3.87	2.47	6.34
HBT	3.60	1.55	5.15

FOX7	2.66	3.23	5.89
NTO	2.27	1.94	4.21
TATB	1.72	2.33	4.05
ATZ	1.49	2.62	4.11
GTZ	1.04	2.94	3.98
AGTZ	2.46	4.41	6.87
DGTZ	1.33	3.20	4.53

8. Calculations at higher order coupling

In order to determine whether increasing the overtone order increases the resolution of predicted up-pumping, we calculated the up-pumping from the overtone 1, overtone 1+2, and the sum of overtones 1-5, Figure S8.1. It is clear that higher order overtones in fact reduce the resolution of prediction.

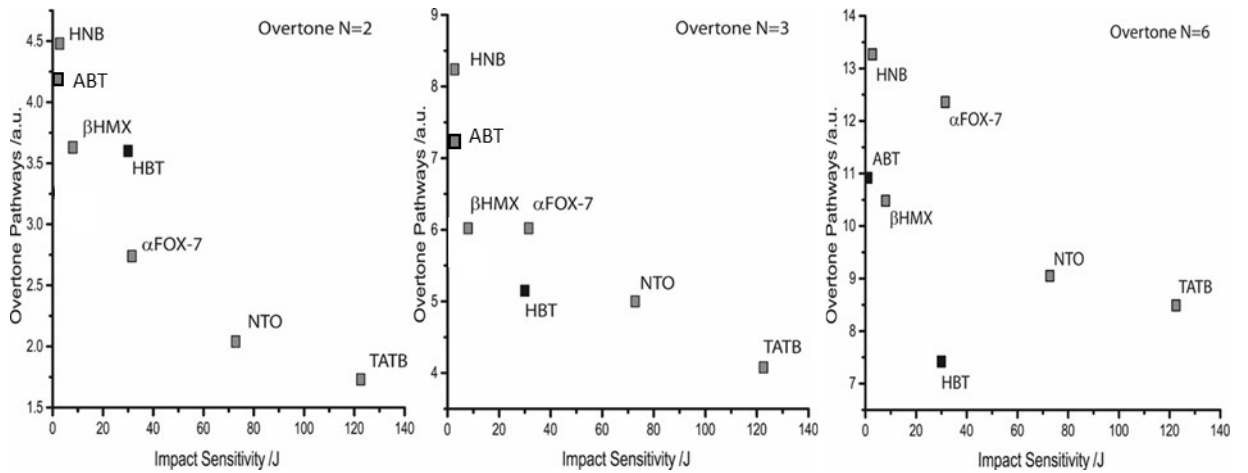


Figure S8.1: Increasing the overtone order for predicted up-pumping. N=2 includes the first overtone, N=3 includes the first and second overtones, and N=6 includes the first five overtone contributions.

9. Vibrational modes of TATB and HNB

Key vibrational modes appear to be wagging and stretching modes of the NO₂ moieties. Thus, pumping excess energy into these modes should be indicative of sensitivity. These modes sit within the doorway region of the highly sensitive HNB molecule, but do not appear within the doorway region of the insensitive TATB species, Table S9.1. Thus, their excitation is considerably higher in HNB.

Table S9.1: Brillouin zone centre (Γ) point vibrational frequencies calculated for TATB and HNB. Dominant mode assignments are made. Values are shown to a maximum of $2\Omega_{max}$. External mode character is denoted X. The value of Ω_{max} is indicated by a dark line. No values are given above $2\Omega_{max}$.

TATB Wavenumber /cm ⁻¹	Dominant Mode Character	HNB Wavenumber /cm ⁻¹	Mode
28.60	X	23.84	X
49.91	X	40.41	X
55.31	X+ring	41.61	X
61.96	X+ring	43.46	X
63.11	X+ring	51.21	-NO ₂ rock + X
84.31	NO ₂ rock t	55.02	-NO ₂ rock + X
85.58	NO ₂ rock	60.29	X
87.25	NO ₂ rock	67.82	-NO ₂ rock + X
93.55	NO ₂ rock	69.25	-NO ₂ rock + X
100.11	X	77.80	-NO ₂ rock
102.41	-NO ₂	78.82	-NO ₂ wag
109.27	X	81.91	X
120.13	X	87.18	X
122.36	-NH ₂ rock	87.64	-NO ₂ rock
129.14	-NH ₂ rock	93.92	X
137.22	-NH ₂ rock	96.83	X
139.93	NH ₂ + NO ₂ rock	97.41	-NO ₂ umbrella
146.11	X	102.75	X
146.23	X	103.76	X
155.92	X	105.94	-NO ₂ rotation
161.73	X + NO ₂ rock	107.74	X
234.80	Umbrella mode	109.23	-NO ₂ rock + X
237.03	Umbrella mode	120.95	-NO ₂ wag

286.04	-NO ₂ rock	121.70	-NO ₂ rock +wag
286.13	-NO ₂ rock	123.46	-NO ₂ rock + X
287.05	-NO ₂ rock	127.42	-NO ₂ wag + X
287.52	-NO ₂ rock	132.04	-NO ₂ rock + X
		160.27	-NO ₂ rock
		167.55	-NO ₂ rock + wag
		168.36	NO ₂ ... NO ₂ bend + rock
		168.82	NO ₂ ... NO ₂ bend + rock
		169.83	NO ₂ ... NO ₂ bend + rock
		170.65	NO ₂ ... NO ₂ bend + rock
		185.60	-NO ₂ wag + rock
		186.47	-NO ₂ wag
		186.78	-NO ₂ wag
		187.22	-NO ₂ wag
		189.17	-NO ₂ wag
		189.29	-NO ₂ wag
		199.89	Ring deformation
		202.12	Ring deformation
		203.68	Ring deformation
		205.44	Ring deformation
		253.06	C-NO ₂ stretch + ring stretch
		253.51	C-NO ₂ stretch + ring stretch
		254.14	C-NO ₂ stretch + ring stretch
		254.74	C-NO ₂ stretch + ring stretch

10. References

- (1) Deschamps, J. R.; Frisch, M.; Parrish, D. Thermal Expansion of HMX. *J. Chem. Crystallogr.* **2011**, *41* (7), 966–970.
- (2) Evers, J.; Klapötke, T. M.; Mayer, P.; Oehlinger, G.; Welch, J. α - and β -FOX-7, Polymorphs of a High Energy Density Material, Studied by X-Ray Single Crystal and Powder Investigations in the Temperature Range from 200 to 423 K. *Inorg. Chem.* **2006**, *45* (13), 4996–5007.
- (3) Bolotina, N. B.; Hardie, M. J.; Speer Jr, R. L.; Pinkerton, A. A. Energetic Materials: Variable-Temperature Crystal Structures of γ - and ϵ -HNIW Polymorphs. *J. Appl. Crystallogr.* **2004**, *37*, 808–814.
- (4) Akopyan, Z. A.; Struchkov, Y. T.; Dashevskii, V. G. Crystal And Molecular Structure of Hexanitrobenzene. *Zh. Strukt. Khim.* **1966**, *7*, 408.
- (5) Klapötke, T. M.; Piercey, D. G. 1,1'-Azobis(Tetrazole): A Highly Energetic Nitrogen-Rich Compound with a N10 Chain. *Inorg. Chem.* **2011**, *50* (7), 2732–2734.
- (6) Klapötke, T. M.; Sabaté, C. M. 5,5'-Hydrazinebistetrazole: An Oxidation-Stable Nitrogen-Rich Compound and Starting Material for the Synthesis of 5,5'-Azobistetrazolates. *Zeitschrift für Anorg. und Allg. Chemie* **2007**, *633* (15), 2671–2677.
- (7) Cady, H. H.; Larson, A. C. The Crystal Structure of 1,3,5-Triamino-2,4,6-Trinitrobenzene. *Acta Crystallogr.* **1965**, *18* (3), 485–496.
- (8) Klapötke, T. M.; Stierstorfer, J. Nitration Products of 5-Amino-1H-Tetrazole and Methyl-5-Amino-1H-Tetrazoles—Structures and Properties of Promising Energetic Materials. *Helv. Chim. Acta* **2007**, *90*, 2132–2150.
- (9) Hinuma, Y.; Pizzi, G.; Kumagai, Y.; Oba, F.; Tanaka, I. Band Structure Diagram Paths Based on Crystallography. *Comput. Mater. Sci.* **2017**, *128*, 140–184.
- (10) Bernstein, J. *Ab Initio* Study of Energy Transfer Rates and Impact Sensitivities of Crystalline Explosives. *J. Chem. Phys.* **2018**, *148* (8), 084502.